8-1-2003

Statistics Of Arctic Cloud Downwelling Infrared Emissivity

Steven P. Neshyba
University of Puget Sound, nesh@pugetsound.edu

Carsten Rathke
Institut für Weltraumwissenschaften, Freie Universität Berlin, Berlin, Germany

Citation

Neshyba, Steven P., and C. Rathke. 2003. "Statistics of Arctic cloud downwelling infrared emissivity." Journal Of Geophysical Research-atmospheres 108(D15): 4468-4468.

Statistics of Arctic cloud downwelling infrared emissivity

Steven P Neshyba
Department of Chemistry, University of Puget Sound, Tacoma, Washington, USA

Carsten Rathke
Institut für Weltraumwissenschaften, Freie Universität Berlin, Berlin, Germany

Received 7 November 2002; revised 20 February 2003; accepted 18 March 2003; published 12 August 2003.

[1] Time series of optical depth of Arctic stratus clouds are investigated for scaling properties and biases with respect to a plane-parallel model. The study is based on 3 years of infrared spectrometer and microwave radiometer measurements made at the Atmospheric Radiation Measurement North Slope of Alaska site. Power spectra of radiance and radiance emissivity are found to indicate scaling with a spectral coefficient on the order of 5/3 over 0.5–10 hours, consistent with the Kolmogorov-Obukhov prediction [*Kolmogorov*, 1941] for three-dimensional turbulence. Irradiance emissivities inferred from the data set, using an independent column approximation and 6-hour time intervals, are further analyzed to find reduction factors for the same mean optical depth in a plane-parallel representation. These factors are estimated to average 0.82 in March and 0.48 in September but with a high degree of variability: The most inhomogeneous quarters of these data sets exhibit reduction factors of 0.57 (March) and 0.20 (September). Observed reduction factors for radiance and irradiance are found to depend primarily on the ratio of mean optical depth to variance, a result consistent with exact results for a γ distribution of cloud thickness. *INDEX TERMS:* 0320 Atmospheric Composition and Structure: Cloud physics and chemistry; 3250 Mathematical Geophysics: Fractals and multifractals; 3332 Meteorology and Atmospheric Dynamics: Mesospheric dynamics; 3360 Meteorology and Atmospheric Dynamics: Remote sensing; *KEYWORDS:* Arctic, cloud, inhomogeneity, radiance

Citation: Neshyba, S. P, and C. Rathke, Statistics of Arctic cloud downwelling infrared emissivity, *J. Geophys. Res.*, *108*(D15), 4468, doi:10.1029/2002JD003157, 2003.

1. Introduction

[2] Characterization of the statistics of horizontal variability of atmospheric properties has been an objective of considerable interest for many years [e.g., *Syroka and Toumi*, 2001; *Ishida*, 1986]. Scaling of cloud liquid water content, for example, has recently been found to span a range from centimeters to kilometers [*Davis et al.*, 1999]. Another statistical approach is the use of distribution functions for representing the horizontal variability of cloud thickness [*Barker and Wielicki*, 1997]. Apart from their fundamental geophysical importance, these characterizations address an increasing need to accurately represent variability within unresolved, subgrid scales of global climate models (GCMs).

[3] In this paper we take a statistical approach to the analysis of thermal radiance emitted downward from Arctic clouds. Our study is motivated by the fact that thermal, i.e., longwave downward radiation, is the dominant source of radiant energy at the surface in the Arctic throughout most of the year [*Curry et al.*, 1996]. Cloudiness can increase the longwave downward irradiance by up to 30% [*Intrieri et al.*, 2002a]. Hence assessing the effect of cloud horizontal variability on the longwave downward irradiance is of considerable interest for modeling the polar climate and sea-ice extent [*Wang and Key*, 2002].

[4] Our study relies primarily on 3 years of downwelling radiance recorded at Barrow, Alaska, by the Atmospheric Radiation Measurement's (ARM) Atmospheric Emitted Radiance Interferometer (AERI) [*Smith et al.*, 1995; *Knuteson et al.*, 1999]. These spectra have a spectral resolution of 0.5 cm^{-1} and are recorded about every 7 min. In section 2, our assumptions relating infrared emissivity and optical depth are presented, along with a bispectral algorithm used to retrieve cloud radiance emissivity and optical depths for clouds of moderate thickness. For thicker clouds, cloud thickness is inferred from ARMs microwave radiometry data over the same time period. The combination is a nearly continuous record of vertically integrated optical depth over a span of 3 years (1999–2001). In section 3, we use power spectra of month-long segments of this data set to identify the time range over which the cloud field exhibits scaling. For moving 6-hour windows, we calculate the mean optical depth, $\langle\delta\rangle$, and a homogeneity parameter, $\nu = (\langle\delta\rangle/\sigma)^2$ (as used by *Barker et al.* [1996]), where σ^2 is the variance δ of for the window. The resulting data set of parameters, spanning 1999–2001, is then used to examine the difference

0148-0227/03/2002JD003157

in irradiance emissivity between observations and plane-parallel cloud geometry, the latter being a common representation in climate models [*Tiedtke*, 1996].

2. Optical Depth and the Bispectral Retrieval Algorithm

[5] The connection between vertically integrated optical depth, δ, and cloud radiance emissivity, ε_{rad}, is provided by the effective emissivity relation [*Rathke and Fischer*, 2002]

$$\varepsilon_{rad} \approx 1 - \exp(-\delta/\cos\theta) \tag{1}$$

where θ is the angle of view with respect to zenith. Here δ and ε_{rad} are wavelength-dependent, as well as functions of time and horizontal coordinates. Equation (1) implicitly accounts for scattering effects and partial cloud cover within a given (narrow) field of view, and therefore, ε_{rad} and δ must be interpreted as an "effective" emissivity and optical depth. They depend on cloud microphysical properties (particle phase and size, water content), as well as macrophysical properties (height and thickness). Here δ, for example, is proportional to the vertically integrated cloud liquid or ice water content, the liquid (or ice) water path (LWP), using the approximation

$$\delta \approx k_{abs}\mathrm{LWP}. \tag{2}$$

At a wavelength of 962 cm^{-1}, a spherical droplet of liquid water with radius 10 μm is predicted by Mie theory to have an absorption coefficient of $k_{abs} = 0.0614\ m^2g^{-1}$ [*Wiscombe*, 1980].

[6] Within a given time window, the radiance emissivity for this zenith angle determines a probability density function for optical depth, $\rho(\delta')$. Then the time average of radiance emissivity is

$$\langle \varepsilon_{rad}(\theta) \rangle = \int_0^\infty \rho(\delta')\left(1 - e^{-\delta'/\cos\theta}\right) d\delta'. \tag{3}$$

The angle brackets indicate an average over a 6-hour window; that is, we assume ergodicity.

[7] The emissivity associated with downwelling hemisphere-integrated radiance, hereafter "irradiance emissivity," is obtained next. We associate with any given zenith angle a vertical optical depth of a single column corrected by $1/\cos\theta$. This is the "independent column approximation" (ICA) [*Ronnholm et al.*, 1980; *Cahalan et al.*, 1994]. The irradiance emissivity is then

$$\langle \varepsilon_{irrad} \rangle = \int_0^{\pi/2} 2\langle \varepsilon_{rad}(\theta) \rangle \sin\theta\cos\theta \; d\theta, \tag{4}$$

where we have assumed $\langle \varepsilon_{rad} \rangle$ does not depend on azimuthal angle.

[8] Averages such as appearing in equation (3) may be taken for observed or model distributions of δ. For example, we define a plane-parallel horizontal (PPH) emissivity average by using a monodispersion for $\rho(\delta')$, so that $\langle \varepsilon_{rad,PPH} \rangle$ is given by equation (1) with $\delta = \langle \delta \rangle$, and

$$\langle \varepsilon_{irrad,PPH} \rangle = 1 - e^{-\langle \delta \rangle}(1 - \langle \delta \rangle) - \langle \delta \rangle^2 Ei(\langle \delta \rangle), \tag{5}$$

where Ei is the exponential integral. In the zero-scattering approximation, equation (5) is approximated as

$$\langle \varepsilon_{irrad,PPH} \rangle \approx 1 - e^{-F\langle \delta \rangle}, \tag{6}$$

where F is the diffusivity factor, 1.66 [*Paltridge and Platt*, 1976].

[9] Regarding the observational record, a first inclination is to use liquid water path values from microwave radiometer measurements [*Liljegren*, 1994] to deduce a cloud's effective emissivity. The ARM data set at Barrow is nearly continuous over the 3 years considered here (1999–2001), recorded at 5-min intervals. Two factors make such an approach incomplete for our purpose, however. First, ice occurs commonly in Arctic clouds, but microwave radiometer retrievals are largely insensitive to ice content. Second, LWP retrievals from microwave radiometry [*Liljegren*, 1994] exhibit high relative errors when cloud thickness is less than 20 g/m^2 [*Dong et al.*, 2000], whereas such clouds are commonplace in the Arctic [e.g., *Curry et al.*, 1996].

[10] Therefore we present here an algorithm for inferring optical depths based on downwelling infrared radiance spectra measured at the North Slope of Alaska (NSA) ARM site by the Atmospheric Emitted Radiance Interferometer (AERI) [*Smith et al.*, 1995; *Knuteson et al.*, 1999]. Figure 1 is presented to show that the influence of clouds in these spectra is most evident in the 8–12 μm (750–1250 cm^{-1}) window, in particular in "microwindows," frequencies between lines of strong radiative emission from gases. Figure 1 also demonstrates the sensitivity of the approach, clearly distinguishing a cloud with $\delta = 0.1$ from another with $\delta = 1.5$ (at 962 cm^{-1}). These optical depths were inferred using a bispectral retrieval algorithm, which we now describe.

[11] Given a cloud temperature T_{cld}, $\delta(x)$ gives rise to a cloud downwelling radiance given by

$$I(\nu) \approx B(\nu, T_{cld})\varepsilon(\nu), \tag{7}$$

received at the ground according to

$$I(\nu) = t(\nu)\left\{B(\nu, T_{cld})\varepsilon(\nu) + B\left(\nu, T_{bkg}\right)[1 - \varepsilon(\nu)]\right\} + B(\nu, T_{atm}) \cdot [1 - t(\nu)], \tag{8}$$

where I is the observed downwelling radiance, $B(\nu, T_{cld})$ is the Planck function at T_{cld}, $t(\nu)$ is the atmospheric transmissivity from the cloud to the surface, T_{atm} is the average temperature of the atmosphere below the cloud, and T_{bkg} is the radiative temperature corresponding to the "background," clear-sky downwelling radiance. (For the remainder of this section "ν" refers to wavenumber).

[12] Figure 2 shows time series of downwelling radiance in the 1233 and 962 cm^{-1} microwindows, expressed in equivalent brightness temperatures. During March 2000, many measurements correspond to clear-sky conditions. These appear as low brightness values, $\sim$180 K in the 1233 cm^{-1} microwindow and $\sim$150 K in the 962 cm^{-1} microwindow. Also shown are clear-sky brightness temperatures in these microwindows, based on the subarctic winter model atmosphere of *McClatchey et al.* [1972]. The approximate agreement (5–10 K root-mean-square error) leads us to the conclusion that "clear-sky" parameters t,

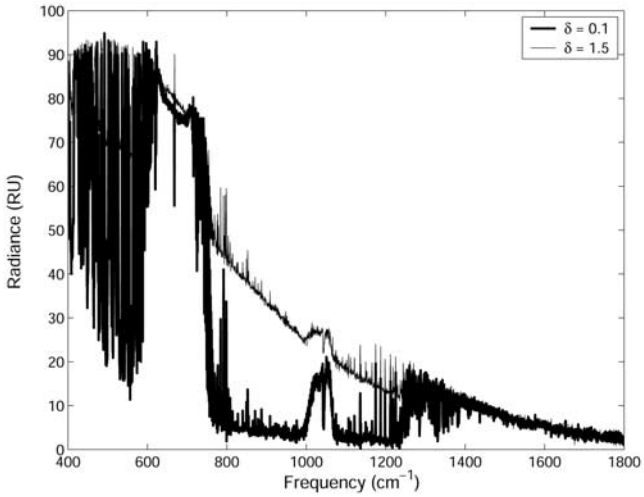

Figure 1. ARM/AERI spectra taken at Barrow, Alaska, on 1 March 2001. The bold line is the spectrum of a cloud with retrieved optical depth of 0.1 at 962 cm^{-1}, taken at 2130 GMT. The thin line is the spectrum of a cloud with retrieved optical depth of 1.5 at 962 cm^{-1}, taken at 0334 GMT. Radiance units are $mW/(m^{-2}\ St\ cm^{-1})$.

T_{bkg}, and T_{atm} derived from the *McClatchey et al.* [1972] model atmosphere are satisfactory throughout the month. Similar comments apply to August, although with less confidence because there are fewer cloudless measurements for comparison.

[13] T_{cld} and ε are inferred from AERI spectra by a simple, bispectral retrieval algorithm. Retrieving T_{cld} and ε from two spectral observations in the thermal infrared window region was first proposed by *Inoue* [1985]. Assuming that t, T_{bkg}, and T_{atm} are known, a retrieval of T_{cld} and ε is possible, if one can find two microwindows (centered at frequencies ν_1 and ν_2) for which $\varepsilon(\nu_1) = \alpha\varepsilon(\nu_2)$, regardless of cloud particle size. While *Inoue* [1985] had to rely on spectral observations prescribed by the specifications of the advanced very high resolution radiometer (AVHRR) satellite instrument, with the continuous spectral record of the AERI spectrometer, it is possible to choose the pair of microwindows best suited for this purpose.

[14] In order to discriminate the pair of microwindows for which the retrieval error for T_{cld} and hence ε is smallest, we consider only the cloud contribution in equation (8), i.e., equation (7), so that we obtain

$$\alpha = \frac{\varepsilon(\nu_1)}{\varepsilon(\nu_2)} = \frac{I(\nu_1)B(\nu_2, T_{cld})}{I(\nu_2)B(\nu_1, T_{cld})} = \text{const}, \tag{9}$$

and, after rearranging,

$$T_{cld} \approx c_2(\nu_2 - \nu_1) \Big/ \ln\left[\frac{1}{\alpha}\frac{I_1}{I_2}\left(\frac{\nu_2}{\nu_1}\right)^3\right]. \tag{10}$$

where c_2 is Planck's second constant. The retrieval error for T_{cld} is thus a function of T_{cld} and ε, ν_1 and ν_2, the noise ΔI_1, and the effective emissivity ratio α and its standard deviation $\Delta\alpha$:

$$\Delta T_{cld} \approx \sqrt{\left(\frac{T_{cld}}{\ln\left[\frac{1}{\alpha}\frac{I(\nu_1)}{I(\nu_2)}\left(\frac{\nu_2}{\nu_1}\right)^3\right]}\frac{\Delta I_1}{I_1}\right)^2 + \left(\frac{T_{cld}}{\ln\left[\frac{1}{\alpha}\frac{I(\nu_1)}{I(\nu_2)}\left(\frac{\nu_2}{\nu_1}\right)^3\right]}\frac{\Delta\alpha}{\alpha}\right)^2}. \tag{11}$$

We have calculated α and $\Delta\alpha$ with the radiative transfer model DISORT [*Stamnes et al.*, 1988] for all microwindows in the 770–2600 cm^{-1} spectral range for the range of cloud/surface temperature contrasts expected in the Arctic spring and summer and for liquid water and ice clouds. The clouds were assumed to be composed of spherical particles, distributed according to a Gamma-Hansen [*Hansen*, 1971] size distribution, characterized by an effective particle radius r_{eff} and an effective variance v_{eff}. Narrow and broad size distributions were considered ($v_{eff} = 0.021$ and $v_{eff} = 0.370$ for liquid water clouds with $r_{eff} = 2, 4, \ldots, 16\ \mu m$, and $v_{eff} = 0.050$ and $v_{eff} = 0.400$ for ice clouds with $r_{eff} = 5, 10, \ldots, 40\ \mu m$).

[15] Having α and $\Delta\alpha$, we have estimated ΔT_{cld} with equation (11) for all pairs of microwindows in the 770–2600 cm^{-1} spectral range. The smallest error was found for $\nu_1 = 962\ cm^{-1}$ and $\nu_2 = 1233\ cm^{-1}$, so that we based our bispectral algorithm on radiance observations in these microwindows. The algorithm consists of two steps: (1) assuming t, $T_{atm,1}$ and $T_{atm,2}$, a primitive atmospheric correction is applied and I' is determined

$$\begin{aligned} I'(\nu_1) &\approx \{I(\nu_1) - [1 - t(\nu_1)]B(\nu_1, T_{atm,1})\}/t(\nu_1) \\ I'(\nu_2) &\approx \{I(\nu_2) - [1 - t(\nu_2)]B(\nu_2, T_{atm,2})\}/t(\nu_2) \end{aligned} \tag{12}$$

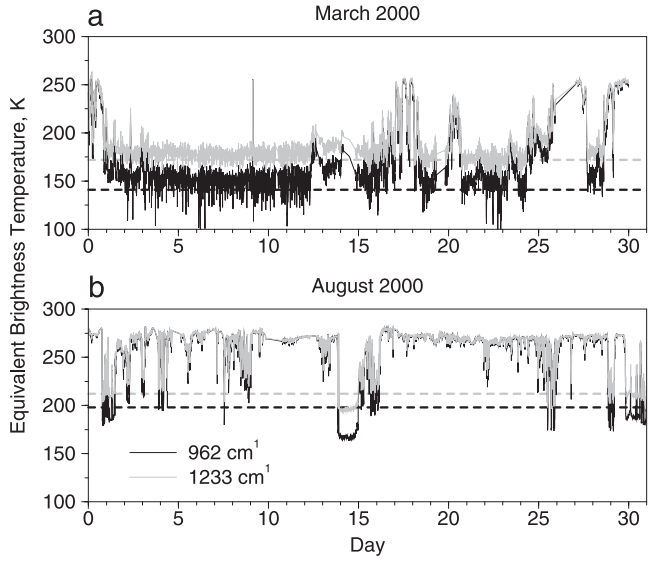

Figure 2. Time series of downwelling infrared radiance (expressed in brightness temperatures) measured by the AERI in (a) March 2000 and (b) August 2000 at the NSA ARM site. Brightness temperatures are averaged over the width of the microwindows centered at 962 cm^{-1} (959.998–964.337 cm^{-1}) and 1233 cm^{-1} (1230.976–1235.316 cm^{-1}). The dotted lines indicate clear-sky T_{bkg} values calculated for these microwindows and the *McClatchey et al.* [1972] (a) subarctic winter and (b) subarctic summer atmospheres. See color version of this figure in the HTML.

Table 1. Parameters for the Bispectral Retrieval Algorithm

	Subarctic Winter Atmosphere		Subarctic Summer Atmosphere	
	ν_1 = 962 cm^{-1}	ν_2 = 1233 cm^{-1}	ν_1 = 962 cm^{-1}	ν_2 = 1233 cm^{-1}
α[a]	0.98 ± 0.04	0.98 ± 0.04	0.97 ± 0.04	0.97 ± 0.04
T_{bkg}, K[b]	130 (100–159)	164 (127–181)	170 (103–238)	191 (131–239)
T[c]	0.98 (1.00–0.96)	0.96 (0.99–0.93)	0.79 (0.98–0.59)	0.82 (0.97–0.66)
T_{atm}, K[d]	252 (248–256)	247 (246.8–247.3)	283 (281–285)	280 (279–281)

[a]Average is given plus/minus standard deviation.
[b]The minimum values correspond to the background radiance at the height of the tropopause (9 km in winter, 10 km in summer). The maximum values correspond to the background radiance at the height of 1 km in these atmospheres but with the water vapor column doubled in all layers.
[c]The minimum values correspond to the transmission from the surface to a height of 1 km in these atmospheres but with the water vapor column halved in all layers. The maximum values correspond to the transmission from the surface to the tropopause in these atmospheres but with the water vapor column doubled in all layers.
[d]The minimum values correspond to the average radiative temperature of these atmospheres from the surface to the tropopause. The maximum values correspond to the average radiative temperature of these atmospheres from the surface to a height of 1 km.

and (2) assuming α, $T_{bkg,1}$ and $T_{bkg,2}$, T_{cld} and $\varepsilon(\nu_1)$ are found so that

$$\frac{I'(\nu_1) - B\left(\nu_1, T_{bkg,1}\right)}{B(\nu_1, T_{cld}) - B\left(\nu_1, T_{bkg,1}\right)} = \varepsilon(\nu_1) = \alpha\varepsilon(\nu_2) = \alpha\frac{I'(\nu_2) - B\left(\nu_2, T_{bkg,2}\right)}{B(\nu_2, T_{cld}) - B\left(\nu_2, T_{bkg,2}\right)}, \quad (13)$$

with $0 < \varepsilon(\nu_1) \leq 1$ and 200 K $< T_{cld} < T_{surf} + 30$ K. The only additional information required is the surface temperature T_{surf}, which is provided in the ARM/AERI data set as ambient air temperature at hatch opening. Any measurement for which the two latter conditions cannot be met is labeled "clear." The parameters needed for the application of this algorithm are supplied in Table 1.

[16] Previously (equation (11)), we neglected errors associated with the atmospheric correction, that is, errors due to errors in the specification of t, T_{bkg} and T_{atm}. More realistic error estimates were obtained by repeating the retrievals with the bispectral algorithm and varying all parameters between their minimum and maximum expected values (Table 1). The results of this error analysis are shown for ν_1 = 962 cm^{-1} in Figure 3. The (maximum) total uncertainty is about 5 K for T_{cld} and about 15% for ε in most cases. The largest errors occur for thin clouds; for this reason, cloudy scenes with retrieved optical depth smaller than about 0.1 (corresponding to emissivity smaller than about 0.1) are excluded from this study, as described in section 3. The uncertainty is larger for the summer case because of the potentially larger errors in the atmospheric correction (larger water vapor content of the atmosphere).

[17] Principal limitations of the method are the assumptions of a single cloud layer, and complete cloud cover within the field of view of the AERI during the time of a measurement (about 1 min.).

[18] To summarize, Figure 4 shows retrieved optical depths using the two algorithms based on the ARM data sets at Barrow. Optical depths derived from microwave radiometry are clearly inadequate for thin clouds, $\delta \approx 0-1$, corresponding to LWP $\approx 0-20$ g/m^2 using equation (2). For medium-thickness clouds, $0.1 > \delta > 3$, the bispectral retrieval algorithm is more reliable, but for yet thinner clouds, limitations of the bispectral algorithm become important. We have therefore merged the two data sets in the following way: For any contiguous time period for which ARM microwave radiometry indicates $\delta > 3$, we use those values for δ. For all other time periods we use AERI-derived values for δ. For any retrieval with $\delta < 0.1$, the optical depth is set to zero.

3. Results and Discussion

[19] Emissivities and temperatures retrieved for two months using the bispectral algorithm are presented in Figure 5. These two months were selected because of a near-continuous record of the ARM/FTIR data set. Qualitatively, it is clear that retrieved emissivities track the radiance very closely, as expected. For August 2000, the variability in retrieved temperature is quite small in relative terms (smaller than 5% of the mean value for the month) compared to the variability of retrieved optical depths, which spans the full physically permissible range (0–1) on an almost daily basis. For March 2001, the variability of temperature is greater but (in relative terms) still much less than the variability of the emissivity.

[20] Power spectra of the downwelling radiance and emissivity are presented in Figure 6. Straight line fits to octave-averaged points appear to indicate scaling over 0.5–10 hours. With the exception of radiance for March 2001, spectral coefficients are within ±0.1 of the Kolmogorov-Obukhov prediction [*Kolmogorov*, 1941] for the density fluctuation of a passive scalar in three-dimensional turbulence, 5/3. It is not known whether the unexpectedly high spectral coefficient for radiance in March 2001 (β_R = 1.93 ± 0.09) is representative of the month; considering that the corresponding emissivity exhibits a significantly lower value (β_ε = 1.76 ± 0.06), a possible explanation is that the radiance power spectrum includes scaling in temperature as well as in optical depth.

[21] In order to simulate a ~200–300 km spatial grid scale of a global climate model, we have broken each monthly data set into 6-hour windows. The windows are advanced in increments of 3 hours, yielding eight values of $\langle\delta\rangle$ and eight values of the homogeneity parameter $\nu = (\langle\delta\rangle/\sigma)^2$ per day. Moreover, windows with $\langle\delta\rangle$ smaller than 0.2 were discarded, so that the analysis would address only detected cloud. Figure 7 is a scatterplot of the March and September data sets, spanning years 1999–2001, processed in this way. Geometric means of these distributions are displayed in Table 2. Although quite broad, the distributions in $\langle\delta\rangle$ for the two months are clearly distin-

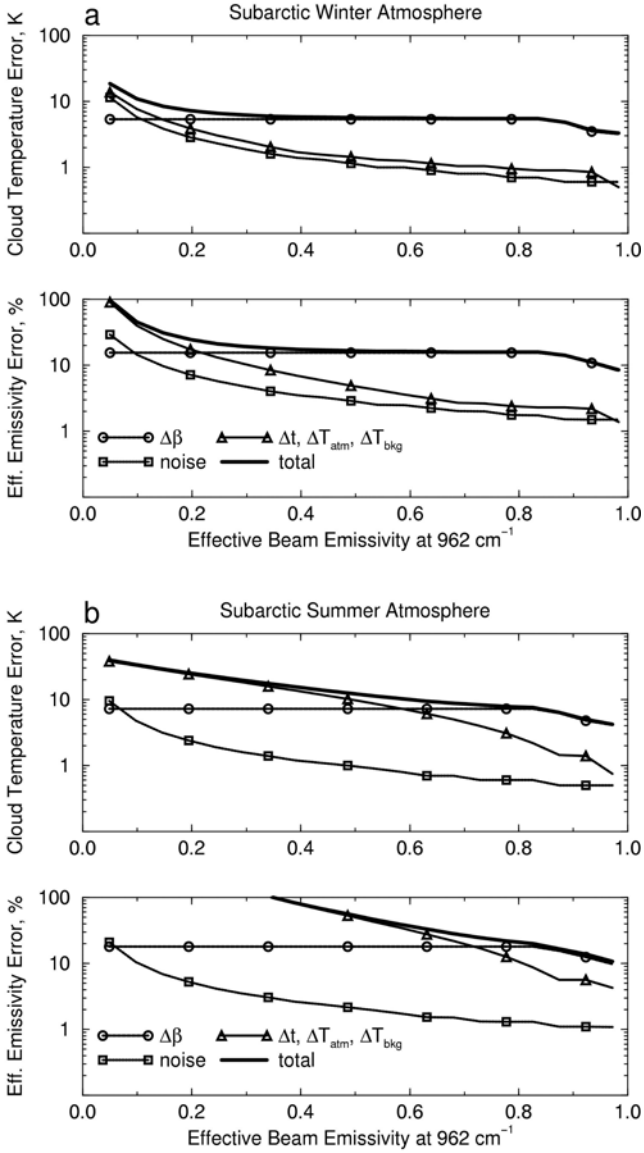

Figure 3. Retrieval error in T_{cld} and $\varepsilon(962\ cm^{-1})$ as a function of $\varepsilon(962\ cm^{-1})$ for the bispectral retrieval algorithm for clouds located in the *McClatchey et al.* [1972] (a) subarctic winter atmosphere and (b) subarctic summer atmosphere. The curves were obtained by varying the different parameters entering equation (8).

guishable from each other, with generally thicker clouds in September. This pattern is consistent with known seasonality of cloudiness in the Arctic (see, e.g., *Intrieri et al.* [2002b] and *Curry et al.* [1996] for recent climatologies]. Figure 7 also suggests that September and March are not nearly so distinguishable in terms of homogeneity as they are in terms of thickness. As Table 2 shows, the geometric mean of the homogeneity parameter for March, $\nu = 3.3$, is slightly higher than for September, $\nu = 2.4$. For comparison, the "overcast stratocumulus" cloud classification of *Barker et al.* [1996] type "A," spans the range $1.5 < \nu < 22$, whereas the "broken stratocumulus classification," type "B", spans $0.4 < \nu < 3$ [*Barker et al.*, 1996].

[22] The distributions in ν displayed in Figure 7 are wide enough to include many 6-hour periods for which clouds are much more inhomogenous, however. Results considering only the most inhomogeneous one fourth of 6-hour measurement periods are displayed in Table 3. These subsets of March and September fall generally inside category "B," broken stratocumulus.

[23] We next direct our attention to reduction factors that should be applied to a plane-parallel representation of cloud within a 6-hour time window which, as stated above, is meant to simulate the horizontal resolution of a typical GCM. Equating the average emissivity to plane-parallel functions of the 6-hour-average optical depth defines a radiance plane-parallel reduction factor, χ_{rad},

$$\chi_{rad} = -\frac{\cos(\theta)}{\langle\delta\rangle}\log(1 - \langle\varepsilon_{rad}\rangle), \tag{14}$$

where $\langle\varepsilon_{rad}\rangle$ is the average radiance emissivity observed or simulated within a given 6-hour time window. For the irradiance reduction factor, χ_{irrad}, we have

$$\chi_{irrad} = \frac{1}{\langle\delta\rangle}\left\langle\varepsilon_{irrad,PPH}\right\rangle^{-1}\langle\varepsilon_{irrad}\rangle, \tag{15}$$

where $\left\langle\varepsilon_{irrad,PPH}\right\rangle^{-1}$ is the inverse of equation (5). In deciding how to display reduction factors obtained according to this definition, it is useful to consider some theoretical results. *Cahalan* [1994] presented an approach in which the reflectivity (or equivalently, the emissivity as given by equation (1)) is written as a Taylor expansion of plane-parallel cloud reflectivity about $\log(\delta)$. The zeroth-order part of that expansion is used to derive an expression for χ for a given cloud thickness distribution, $\rho(\delta')$. For the bounded cascade model, for example, this approach produces the functional equivalent of $\chi_{rad} = f(\nu)$ (omitting, notationally, dependence of the bounded cascade parameter "c," which

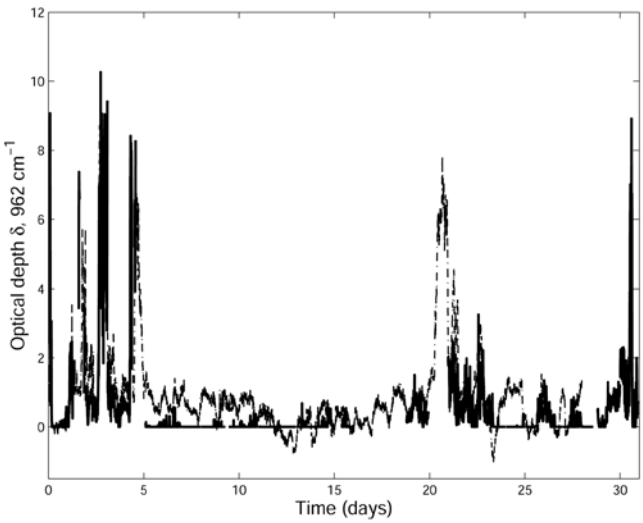

Figure 4. Optical depths at 962 cm^{-1} retrieved from downwelling infrared radiance data according to the bispectral algorithm (solid line), and microwave data, based on ARM/MWR retrievals of LWP [*Liljegren*, 1994] (dashed-dotted) during March 2001. The origin is midnight of March 1, 2001 (GMT).

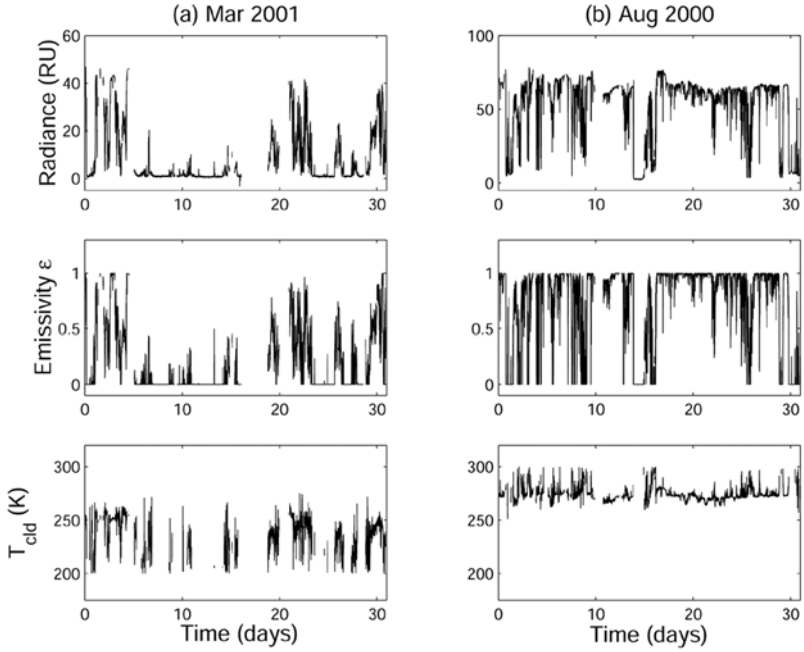

Figure 5. Recorded radiance, retrieved emissivity, and retrieved cloud temperature for selected months in 1998–2001. The origin in each graph is midnight GMT of the first of the month. Emissivities correspond to a frequency of 962 cm^{-1}.

determines the spectral coefficient) [*Cahalan*, 1994, equation (B2)]. Another distribution function is the γ distribution,

$$\rho(\delta) = \frac{1}{\Gamma(\nu)} \left(\frac{\nu}{\langle\delta\rangle}\right)^{\nu} \delta^{\nu-1} \exp\left(-\nu \frac{\delta'}{\langle\delta\rangle}\right) \tag{16}$$

[*Barker*, 1996]. Cahalan's zeroth-order approach to the γ distribution also produces the functionality $\chi_{rad} = f(\nu)$,

$$\chi_{rad,\gamma 0} = \prod_{k=0}^{\infty} \left(1 + \frac{1}{\nu + k}\right) \exp\left(-\frac{1}{\nu + k}\right) \tag{17}$$

[*Barker*, 1996].

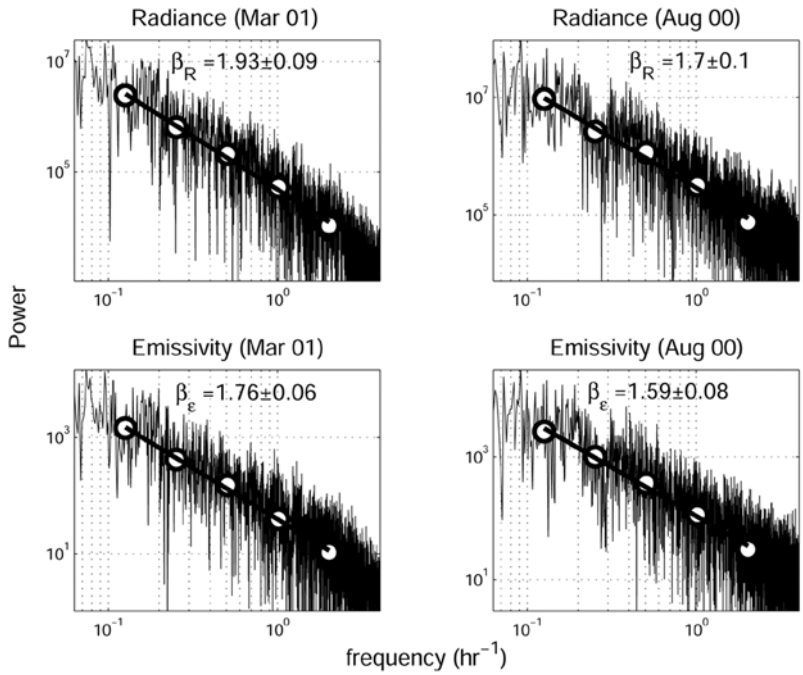

Figure 6. Power spectra of the radiance and emissivity appearing in Figure 5. Straight lines are fit to octave-averaged data points. Uncertainties are at the 95% confidence level based on deviations of these points from the best fit straight line shown.

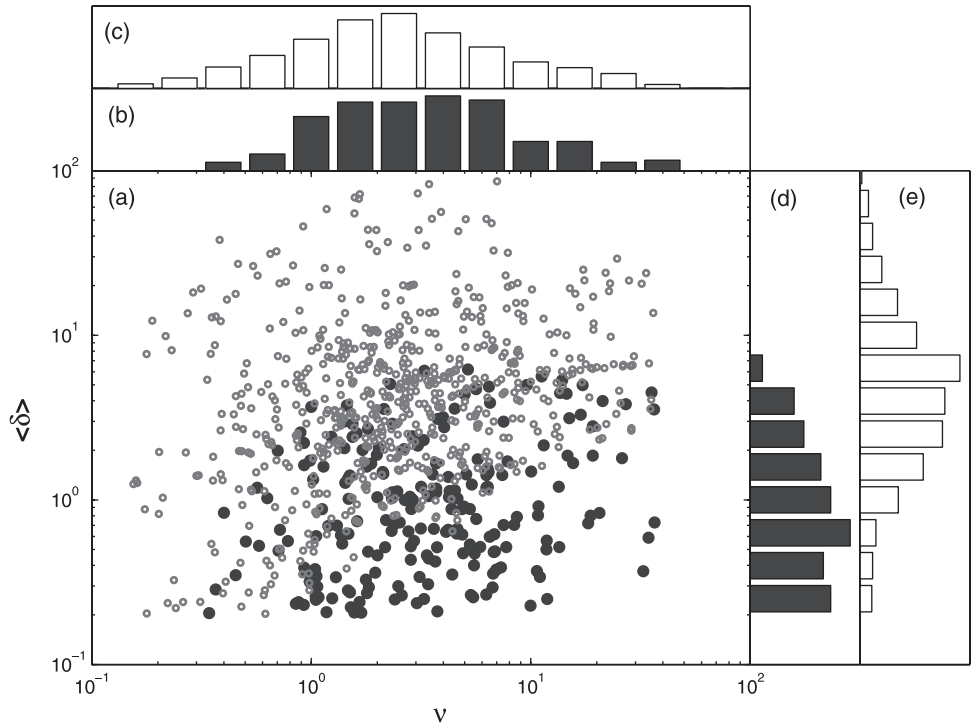

Figure 7. (a) Scatterplot of observed values of mean optical depth, $\langle\delta\rangle$, and homogeneity parameter, ν, for September (open circles) and March (solid circles) 1999–2001 at Barrow. Log-binned histograms for (b) ν, March; (c) ν, September; (d) $\langle\delta\rangle$ March; and (e) $\langle\delta\rangle$, September. See color version of this figure in the HTML.

[24] Exact relationships, not using the zeroth-order approach, are obtainable using numerical and analytical methods. For example, numerical realizations of the bounded cascade model (BCM) in optical depth lead to $\langle\varepsilon_{rad,BCM}\rangle$ using equation (3) and to $\chi_{rad,BCM}$ using equation (14). Alternatively, analysis of the γ distribution of equation (16) leads to the exact result,

$$\chi_{rad,\gamma} = \frac{\nu\cos\theta}{\langle\delta\rangle}\log\left(1+\frac{\langle\delta\rangle}{\nu\cos\theta}\right). \tag{18}$$

That is, unlike the zeroth-order prediction, functionality of the form $\chi_{rad} = \chi_{rad}[(\nu\cos\theta)/\langle\delta\rangle]$ is suggested. Consequently, we have chosen to display in Figure 8 reduction factors as a function of the ratio $\nu/\langle\delta\rangle$ ($\cos\theta = 1$ for these measurements). Also shown are exact analytical results for a γ distribution, equation (18), and exact numerical results for the bounded cascade model, obtained as described above. Although there is considerable scatter, the trend is clearly one that favors the γ distribution, for which the root-mean-square error in χ is 0.07. We also display reduction factors based on the zeroth-order approximation for the γ distribution, equation (17); this function is graphed assuming $\langle\delta\rangle = 4$, but the overall match to observations is no better at other values. Using the ratio of geometric-mean values of ν and $\langle\delta\rangle$ from Tables 2 and 3, equation (18) allows us to infer corresponding reduction factors, also presented in Tables 2 and 3.

[25] Using the zero-scattering approximation (equation (6)) in equation (15), the reduction factor for irradiance also appears as an exclusive function of $\nu/\langle\delta\rangle$,

$$\chi_{irrad,\gamma} \approx \frac{\nu}{F\langle\delta\rangle}\log\left(1+\frac{F\langle\delta\rangle}{\nu}\right). \tag{19}$$

with γ function and zero-scattering approximated. This function is displayed in Figure 9 along with observations. Observations deviate from equation (19) with a root-mean-square error of 0.08.

4. Conclusions

[26] We have analyzed time series of Arctic cloud optical depth, determined from AERI and microwave radiometer

Table 2. Cloud Statistics for 1999–2001

	ν[a]	$\langle\delta\rangle$[b]	χ_{rad}[c]	ε_{rad}, % error	χ_{irrad}[d]	ε_{irrad}, % error
September	2.4	4.0	0.59	8	0.48	4
March	3.3	0.9	0.88	8	0.82	6

[a]Value is geometric mean of 6-hour homogeneity values (ν).
[b]Value is geometric mean of 6-hour mean optical depth values ($\langle\delta\rangle$).
[c]Value is based on the ratio of geometric means ($\nu/\langle\delta\rangle$) and equation (18).
[d]Value is based on the ratio of geometric means ($\nu\langle\delta\rangle$) and equation (19).

Table 3. Cloud Statistics for 1999–2001, Most Inhomogeneous Quarters

	ν[a]	$\langle\delta\rangle$[b]	χ_{rad}[c]	ε_{rad}, % error	χ_{irrad}[d]	ε_{irrad}, % error
September	1.1	8.9	0.27	10	0.20	4
March	1.4	1.5	0.68	22	0.57	13

[a]Value is geometric mean of 6-hour homogeneity values (ν).
[b]Value is geometric mean of 6-hour mean optical depth values ($\langle\delta\rangle$).
[c]Value is based on the ratio of geometric means ($\nu/\langle\delta\rangle$) and equation (18).
[d]Value is based on the ratio of geometric means ($\nu/\langle\delta\rangle$) and equation (19).

measurements made at the ARM NSA site, in order to investigate the impact of horizontal cloud inhomogeneity on downward longwave radiation, an important variable for polar climate. The horizontal variability of cloud thickness retrieved from the measurements leads to irradiance plane-parallel reduction factors (χ_{irrad}) of 0.48 typical of September, and 0.82 typical of March, based on 6-hour time windows, using the independent column approximation. The range of reduction factors is quite large, with the most horizontally inhomogeneous quarter exhibiting reduction factors as low $\chi_{irrad} \sim 0.2$ (for September). Observed reduction factors, also calculated within the ICA, compare favorably with exact values based on the γ distribution, with root-mean-square deviations of 0.07–0.08.

[27] The corresponding irradiance emissivity biases are on the order 4–13%. For comparison with actual irradiance values, *Intrieri et al.* [2002a] showed that the net surface cloud radiative forcing at the SHEBA ice camp during the winter of 1998 averaged about 20 W m^{-2} during that time, with an uncertainty of 15%. During a 3-day period in April 1998 reported by *Intrieri et al.* [2002a], the downwelling longwave irradiance attributable to clouds reached a maximum of 60 W m^{-2}, which is about 25% of the total longwave downward irradiance. Thus biases of 13% in this cloud forcing should not be neglected.

[28] Considering cloud optical depth as a proxy for cloud thickness, these results argue for inclusion in climate models of the radiative effects of cloud horizontal variability in a way that depends on the ratio $\nu/\langle\delta\rangle$ (or equivalently, $\langle\delta\rangle/\sigma^2$). Presently, climate models either ignore subgrid cloud variability or use a constant reduction factor for all types of clouds [*Tiedtke*, 1996]. If a climate model were to predict the variance (σ^2) as well as mean ($\langle\delta\rangle$) of cloud thickness for a given grid cell, Figure 9 could provide a useful indication of the irradiance reduction factor likely to occur, as well as the uncertainty in that value.

[29] We should qualify these conclusions by restating approximations or assumptions that might be relevant. First, estimates of the plane-parallel bias made in section 3 are based on an ergodic assumption, that statistics in time are the same as statistics in space. To address to this objection, one would need ground-based spatiotemporal information not available in the ARM/AERI/MWR archive for Barrow. Second, the ICA is applied throughout. Finally, considering that cloud temperature usually shows much less horizontal variability than cloud optical depth [*Rathke et al.*, 2002] (see also Figure 5), it can be expected that these results will not be affected greatly by inclusion of temperature variability. However, we have not undertaken a quantitative examination of this statement.

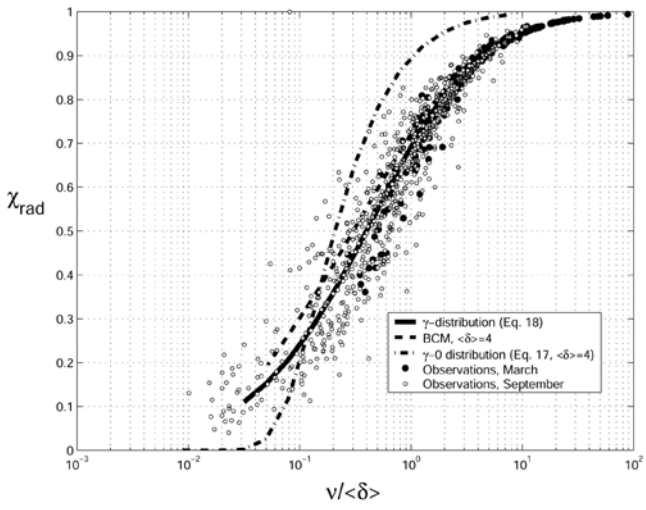

Figure 8. Reduction factors for radiance emissivity, χ_{rad}.

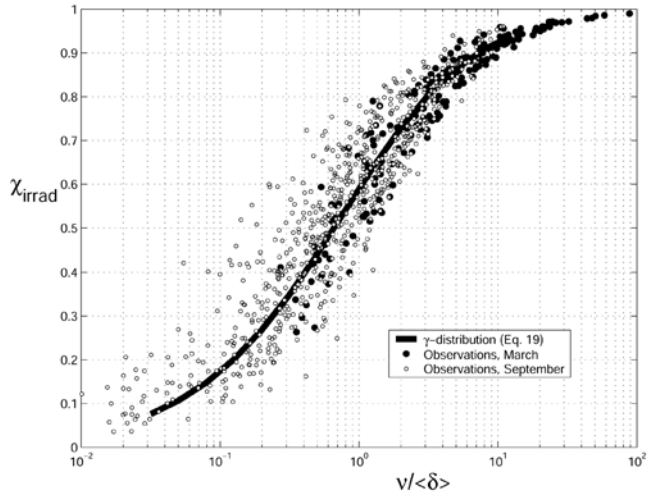

Figure 9. Reduction factors for irradiance emissivity, χ_{irrad}.

[30] **Acknowledgments.** Data were obtained from the Atmospheric Radiation Measurement (ARM) Program sponsored by the U.S. Department of Energy, Office of Science, Office of Biological and Environmental Research, Environmental Sciences Division. SPN gratefully acknowledges support from the International Arctic Research Center. The authors also gratefully acknowledge the comments of anonymous reviewers.

References

Barker, H. W., A parameterization for computing grid-averaged solar irradiances for inhomogeneous marine boundary layer clouds. part I: Methodology and homogeneous biases, *J. Atmos. Sci.*, *53*, 2289–2303, 1996.

Barker, H. W., and B. A. Wielicki, Parameterizing grid-averaged longwave irradiances for inhomogeneous marine boundary layer clouds, *J. Atmos. Sci.*, *54*, 2785–2798, 1997.

Barker, H. W., B. A. Wielicki, and L. Parker, A parameterization for computing grid-averaged solar irradiances for inhomogeneous marine boundary layer clouds. part II: Validation using satellite data, *J. Atmos. Sci.*, *53*, 2304–2316, 1996.

Cahalan, R. F., Bounded cascade clouds: Albedo and effective thickness, *Nonlinear Processes Geophys.*, *1*, 156–167, 1994.

Cahalan, R. F., W. Ridgway, W. J. Wiscombe, S. Golmer, and Harshvardhan, Independent pixel and Monte Carlo estimates of stratocumulus albedo, *J. Atmos. Sci.*, *51*, 3776–3790, 1994.

Curry, J. A., W. B. Rossow, D. Randall, and J. L. Schramm, Overview of Arctic cloud and radiation characteristics, *J. Clim.*, *9*, 1731–1764, 1996.

Davis, A. B., A. Marshak, H. Gerber, and W. J. Wiscombe, Horizontal structure of marine boundary layer clouds from centimeter to kilometer scales, *J. Geophys. Res.*, *104*, 6123–6144, 1999.

Dong, X., P. Minnis, T. P. Ackerman, E. E. Clothiaux, G. G. Mace, C. N. Long, and J. C. Liljegren, A 25-month database of stratus cloud properties generated from ground-based measurements at the ARM SGP site, *J. Geophys. Res.*, *105*, 4529–4538, 2000.

Hansen, J. E., Multiple scattering of polarized light in a planetary atmosphere. part II: Sunlight reflected by terrestrial water clouds, *J. Atmos Sci.*, *28*, 1400–1426, 1971.

Inoue, T., On the temperature and effective emissivity determination of semitransparent cirrus clouds by bispectral measurements in the 10 μm window region, *J. Meteorol. Soc. Jpn.*, *63*, 88–98, 1985.

Intrieri, J. M., J. D. Shupe, T. Uttal, and B. J. McCarty, An annual cycle of Arctic cloud characteristics observed by radar and lidar at SHEBA, *J. Geophys. Res.*, *107*(C10), 8030, doi:10.1029/2000JC000423, 2002a.

Intrieri, J. M., C. W. Fairall, M. D. Shupe, P. O. G. Persson, E. L. Andreas, P. S. Guest, and R. E. Moritz, An annual cycle of Arctic surface cloud forcing at SHEBA, *J. Geophys. Res.*, *107*(C10), 8039, doi:10.1029/2000JC000439, 2002b.

Ishida, H., Mesoscale spatial and temporal variability of meteorological observations from an array of buoys in JASIN-1978, *Boundary Layer Meteorol.*, *37*, 149–165, 1986.

Knuteson, R. O., H. E. Revercomb, F. A. Best, R. G. Dedecker, R. G. Garcia, H. B. Howell, D. C. Tobin, and V. P. Walden, AERI observations at the ARM SGP, NSA, and TWP CART sites, paper presented at Ninth ARM Science Team Meeting, San Antonio, Tex., 1999.

Kolmogorov, A. N., Local structure of turbulence in an incompressible liquid for very large Reynolds numbers, *Dokl. Akad. Nauk SSSR*, *30*(4), 299–303, 1941.

Liljegren, J. C., Two-channel microwave radiometer for observations of total column precipitable water vapor and cloud liquid water path, paper presented at Fifth Symposium on Global Change Studies, Am. Meteorol. Soc., Nashville, Tenn., 1994.

McClatchey, R. A., R. W. Fenn, J. E. A. Selby, F. E. Volz, and J. S. Goring, Optical properties of the atmosphere, *Environ. Res. Pap. 411*, 108 pp., Air Force Geophys. Lab., Hanscom AFB, Mass., 1972.

Paltridge, G. W., and C. M. R. Platt, *Radiative Processes in Meteorology and Climatology*, 318 pp., Elsevier Sci., New York, 1976.

Rathke, C., and J. Fischer, Efficient parameterization of the infrared effective beam emissivity of semitransparent atmospheric layers, *J. Geophys. Res.*, *107*(D4), 4035, doi:10.1029/2001JD000596, 2002.

Rathke, C., S. P. Neshyba, M. Shupe, P. Rowe, and A. Rivers, Radiative and microphysical properties of Arctic stratus clouds from multiangle downwelling infrared radiances, *J. Geophys. Res.*, *107*(D23), 4703, doi:10.1029/2001JD001545, 2002.

Ronnholm, K., M. B. Baker, and H. Harrison, Radiative transfer through media with uncertain or variable parameters, *J. Atmos. Sci.*, *37*, 1279–1290, 1980.

Smith, W. L., H. E. Revercomb, R. O. Knuteson, F. A. Best, R. Dedecker, H. B. Howell, and H. M. Woolf, Cirrus cloud properties derived from high spectral resolution infrared spectrometry during FIRE II. part I: The high resolution interferometer sounder (HIS) systems, *J. Atmos. Sci.*, *52*, 4238–4245, 1995.

Stamnes, K., S.-C. Tsay, W. Wiscombe, and K. Jayaweera, Numerically stable algorithm for discrete-ordinate-method radiative transfer in multiple scattering and emitting layered media, *Appl. Opt.*, *27*, 2502–2509, 1988.

Syroka, J., and R. Toumi, Scaling and persistence in observed and modelled surface temperature, *Geophys. Res. Lett.*, *28*, 3255–3258, 2001.

Tiedtke, M., An extension of cloud-radiation parameterization in the ECMWF model: The representation of subgrid-scale variations of optical depth, *Mon. Weather Rev.*, *124*, 745–750, 1996.

Wang, X. J., and J. R. Key, Aggregate-area radiative irradiance biases, *Ann. Glaciol.*, *34*, 101–105, 2002.

Wiscombe, W. J., Improved Mie scattering algorithms, *Appl. Opt.*, *19*, 1505–1509, 1980.

S. P Neshyba, Department of Chemistry, University of Puget Sound, 1500 N. Warner, Tacoma, WA 98416, USA. (nesh@ups.edu)

C. Rathke, Institut für Weltraumwissenschaften, Freie Universität BerlinCarl-Heinrich-Becker-Weg 6-10, D-12165 Berlin, Germany. (carsten.rathke@de.abb.com)